

Equivalent photons in proton-proton and ion-ion collisions at the LHC

M. I. Vysotsky ^{*1,2,3} and E. V. Zhemchugov ^{†1,3}

¹*Institute for Theoretical and Experimental Physics, 117218, Moscow, Russia*

²*National Research University Higher School of Economics, 101978, Moscow, Russia*

³*Moscow Engineering Physics Institute, 115409, Moscow, Russia*

Abstract

Equivalent photon approximation is used to calculate fiducial cross sections for dimuon production in ultraperipheral proton-proton and lead-lead collisions. Analytical formulae taking into account experimental cuts are derived. The results are compared with the measurements reported by the ATLAS collaboration.

1 Introduction

This year we celebrate the 111th anniversary of L. D. Landau. This paper is devoted to the modern state of the problem first considered by L. D. Landau and E. M. Lifshitz in 1934 when they calculated the production cross section of e^+e^- pair in ultrarelativistic heavy ions collisions [1]. We will demonstrate that this problem is still of great interest.

In spite of many efforts, no New Physics has been found at the LHC so far. It might be a good time to consider scenarios of appearance of New Physics at the LHC that were less attractive at the time when the LHC was under construction. Although the LHC was conceived as a hadron-hadron collider, it also acts as a photon-photon collider with the photons appearing in ultraperipheral collisions of hadrons. This idea is quite old, and it was thoroughly considered during the construction and operation of the RHIC and the LHC [2–16]. However, since hadronic interactions were more likely to deliver the signal of New Physics, particularly in Higgs boson properties, they received more attention in the literature and were given higher priority in the LHC schedule. With the long shutdown of the LHC beginning at the end of 2018, it might be a good time to reconsider photon-photon collisions at the LHC as a source of possible New Physics events so that the necessary detectors adjustments could be made and, perhaps, more time for heavy ions collisions could be negotiated in the LHC schedule.

The leading order Feynman diagram for an ultraperipheral collision is presented in Fig. 1 where instead of lead nuclei there could be any charged particles. The distinctive signature of an ultraperipheral collision is that the charged particles remain intact after the collision. These particles won't have high transverse momentum, so they are difficult to detect with just the main detectors of the ATLAS and CMS experiments, but there exist additional detectors at low scattering angles (the ATLAS forward proton detector [17] and the CMS-TOTEM precision proton spectrometer [18]). However, even without the forward detectors, ultraperipheral collisions manifest through production of particles.

Let us compare proton-proton and lead-lead ultraperipheral collisions as possible sources of New Physics events. Integrated luminosity delivered by the LHC in Run 2 in proton-proton collisions is over 150 fb^{-1} both for the ATLAS and the CMS experiments. Integrated luminosity delivered by the LHC in lead-lead collisions in the heavy ions run was 0.7 nb^{-1} in 2015 [21] and 1.8 nb^{-1} in 2018 [19]. Cross section for an ultraperipheral collision is proportional to Z^4 where Z is the particle charge. For Pb, $Z = 82$, so we get that if there exists New Physics that appears in $\gamma\gamma$ collisions, there will be $(150 \text{ fb}^{-1})/(82^4 \cdot 2.5 \text{ nb}^{-1}) \approx 1.3$ times more events of it during the whole Run 2 pp collisions than there were during the whole heavy ions run. However, Run 2 duration was over 500 days (not counting the 2015 when only 4.2 fb^{-1} were delivered in pp collisions), while the heavy ions run has lasted about 20 days in 2015 and 25 days in 2018. The Z^4 enhancement of the cross section makes the search of New Physics in ultraperipheral collisions of heavy ions at the LHC to look very promising.

The common approach to calculate cross sections of particles production in ultraperipheral collisions is to use the equivalent photon approximation (EPA) [1, 22–24] (see also [25–28]). To compare the result with the experimental data, fiducial cross section has to be calculated, which is the total cross section after applying the

*vysotsky@itep.ru

†zhemchugov@itep.ru

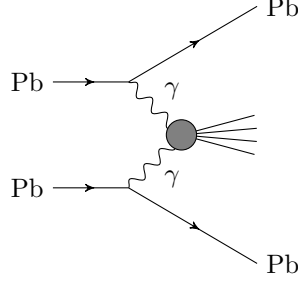


Figure 1: Feynman diagram for an ultraperipheral lead-lead collision.

experimental cuts on the phase space designed to reduce the background and to take into account detector blind spots. The fiducial cross section is usually calculated from the total cross section with the help of the Monte Carlo method (see, e.g., the **SuperCHIC** MC generator [29]). The equivalent photon approximation makes it possible to apply the most common experimental cuts analytically, so often no Monte Carlo method is required.

In this paper, the equivalent photon approximation is used to calculate the cross section of the $pp(\gamma\gamma) \rightarrow pp\mu^+\mu^-$ reaction. Then three kinds of experimental cuts are applied in succession:

1. The cut on the invariant mass of muon pair \sqrt{s} : $\hat{s}_{\min} < s < \hat{s}_{\max}$.
2. The cut on muon transverse momentum p_T : $p_T > \hat{p}_T$.
3. The cut on muon pseudorapidity η : $|\eta| < \hat{\eta}$.

Numerical values of these cuts vary from experiment to experiment and from measurement to measurement. The result of the calculation is used to obtain the theoretical description for the experimental values provided by the ATLAS collaboration [30]. In this measurement, \hat{s}_{\min} was chosen to be 12 GeV to avoid contributions from vector meson decays into $\mu^+\mu^-$ (the heaviest of vector mesons belong to the Υ family); $\hat{s}_{\max} = 70$ GeV; \hat{p}_T is 6 or 10 GeV depending on the invariant mass; $\hat{\eta}$ is 2.4 so that the muon will hit the muon spectrometer.

The same formulae are used to calculate the fiducial cross section for the reaction $\text{Pb Pb } (\gamma\gamma) \rightarrow \text{Pb Pb } \mu^+\mu^-$ studied in Ref. [31].

2 Cross section of the $\mu^+\mu^-$ production without cuts

The distribution of equivalent photons generated by a moving particle with the charge Ze is

$$n(\vec{q})d^3q = \frac{Z^2\alpha}{\pi^2} \frac{\vec{q}_\perp^2}{\omega q^4} d^3q = \frac{Z^2\alpha}{\pi^2\omega} \frac{\vec{q}_\perp^2}{(\vec{q}_\perp^2 + (\omega/\gamma)^2)^2} d^3q, \quad (1)$$

where q is the photon 4-momentum, \vec{q}_\perp is its transverse component, ω is the photon energy, γ is the Lorentz factor of the particle. For a proton with the energy $E = 6.5$ TeV, $\gamma = E/m_p \approx 6.93 \cdot 10^3$. To obtain the equivalent photon spectrum, one has to integrate this expression over the transverse momentum up to some value \hat{q} . The value of \hat{q} should be chosen so that the parent particle does not break apart when emitting a photon of such momentum. For the proton, $\hat{q} = 0.20$ GeV (see Appendix A for derivation). Hence, the equivalent photon spectrum is

$$n(\omega)d\omega = \frac{2Z^2\alpha}{\pi} \ln\left(\frac{\hat{q}\gamma}{\omega}\right) \frac{d\omega}{\omega} \quad (2)$$

in the limit $\omega \ll \hat{q}\gamma$. This simple expression allows us to obtain analytical formulas for the cross section of muon pair production with the experimental cuts.

Muon pair production in ultraperipheral proton-proton collisions in the leading order is described by the Feynman diagrams in Fig. 2. The corresponding cross section is

$$\sigma(pp(\gamma\gamma) \rightarrow pp\mu^+\mu^-) = \int_{m_\mu^2/\hat{q}\gamma}^{\hat{q}\gamma} d\omega_1 \int_{m_\mu^2/\omega_1}^{\hat{q}\gamma} d\omega_2 \sigma(\gamma\gamma \rightarrow \mu^+\mu^-) n(\omega_1) n(\omega_2), \quad (3)$$

where ω_1 and ω_2 are the photon energies and $\sigma(\gamma\gamma \rightarrow \mu^+\mu^-)$ is the Breit-Wheeler cross section [32]:

$$\sigma(\gamma\gamma \rightarrow \mu^+\mu^-) = \frac{4\pi\alpha^2}{s} \left[\left(1 + \frac{4m_\mu^2}{s} - \frac{8m_\mu^4}{s^2}\right) \ln \frac{1 + \sqrt{1 - 4m_\mu^2/s}}{1 - \sqrt{1 - 4m_\mu^2/s}} - \left(1 + \frac{4m_\mu^2}{s}\right) \sqrt{1 - \frac{4m_\mu^2}{s}} \right], \quad (4)$$

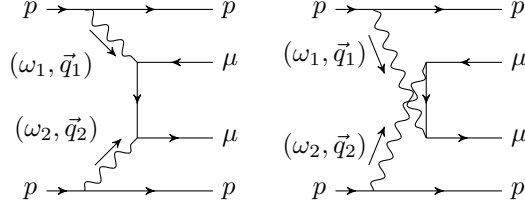


Figure 2: Leading order Feynman diagrams for the $pp(\gamma\gamma) \rightarrow pp\mu^+\mu^-$ reaction.

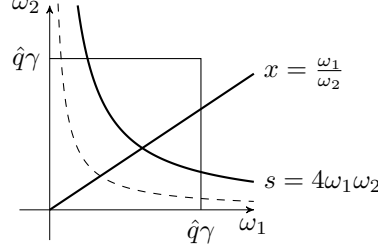


Figure 3: Integration domain of (3). The dashed line corresponds to $s = 4m_\mu^2$. The domain is above the dashed line and inside the square.

$s = 4\omega_1\omega_2$ is the invariant mass of the muons. The integration domain of (3) is presented in Fig. 3. It is convenient to change the integration variables from ω_1, ω_2 to s and x where $x = \omega_1/\omega_2$. Then the integration can be rearranged as follows:

$$\begin{aligned} \sigma(pp(\gamma\gamma) \rightarrow pp\mu^+\mu^-) &= \int_{(2m_\mu)^2}^{(2\hat{q}\gamma)^2} ds \sigma(\gamma\gamma \rightarrow \mu^+\mu^-) \int_{s/(2\hat{q}\gamma)^2}^{(2\hat{q}\gamma)^2/s} \frac{dx}{8x} n\left(\sqrt{\frac{sx}{4}}\right) n\left(\sqrt{\frac{s}{4x}}\right) \\ &= \frac{\alpha^2}{2\pi^2} \int_{(2m_\mu)^2}^{(2\hat{q}\gamma)^2} \frac{ds}{s} \sigma(\gamma\gamma \rightarrow \mu^+\mu^-) \int_{s/(2\hat{q}\gamma)^2}^{(2\hat{q}\gamma)^2/s} \frac{dx}{x} \ln \frac{(2\hat{q}\gamma)^2}{sx} \ln \left[\frac{(2\hat{q}\gamma)^2}{s} \cdot x \right] \end{aligned} \quad (5)$$

(note the symmetry of the integral under the $x \rightarrow 1/x$ replacement). Thus, we get

$$\sigma(pp(\gamma\gamma) \rightarrow pp\mu^+\mu^-) = \frac{16\alpha^2}{3\pi^2} \int_{(2m_\mu)^2}^{(2\hat{q}\gamma)^2} \frac{ds}{s} \sigma(\gamma\gamma \rightarrow \mu^+\mu^-) \ln^3 \frac{2\hat{q}\gamma}{\sqrt{s}}. \quad (6)$$

Since $\sigma(\gamma\gamma \rightarrow \mu^+\mu^-)$ falls as $1/s$ for $s \gg 4m_\mu^2$, in the leading logarithmic approximation the logarithm in this expression should be taken at $s = 4m_\mu^2$. Then¹

$$\sigma(pp(\gamma\gamma) \rightarrow pp\mu^+\mu^-) = 8 \cdot \frac{28}{27} \frac{\alpha^4}{\pi m_\mu^2} \ln^3 \frac{\hat{q}\gamma}{m_\mu}. \quad (7)$$

In this formula, when the masses of the produced particles m are considerably less than \hat{q} , the latter should be replaced with m .² This is precisely the case of the cross section for e^+e^- pair production considered in Ref. [1]. Another difference from Eq. (37) in Ref. [1] is that Ref. [1] considers the collision in the laboratory frame where the nucleus is at rest and $\gamma \equiv \gamma_{c.m.s.} = (\gamma_{lab}/2)^{1/2}$.

For a proton-proton collision at the LHC with the energy of 13 TeV,

$$\sigma(pp(\gamma\gamma) \rightarrow pp\mu^+\mu^-) \approx 0.22 \mu\text{b}. \quad (8)$$

¹ An incorrect spectrum of equivalent photons was used in [33, Eq. (1.4)] ($\ln^2(E/m_e)$ should be replaced with $\ln(E/\omega_1)\ln(E/\omega_2)$ inside the integral), which resulted into an extra factor of $3/2$ in Eq. (5.4) and note [23] in the same paper. This error was later propagated into [26, Eq.(5.4)]. See [28, the second footnote on page 256] for the discussion of similar errors often occurring in the applications of the equivalent photon approximation.

²In the case of τ -leptons production, the factor \hat{q}/m_τ remains and suppresses the cross section.

3 Cross section of the $\mu^+\mu^-$ production with experimental cuts

3.1 Cut on the invariant mass of the $\mu^+\mu^-$ pair

The cut on the invariant mass is trivial to apply: only the limits of the integration over s in (5) have to be changed. For $(2m_\mu)^2 \leq \hat{s}_{\min} < s < \hat{s}_{\max} \leq (2\hat{q}\gamma)^2$,

$$\sigma_{\text{fid.}}^{(\hat{s})}(pp(\gamma\gamma) \rightarrow pp\mu^+\mu^-) = \int_{\hat{s}_{\min}}^{\hat{s}_{\max}} ds \sigma(\gamma\gamma \rightarrow \mu^+\mu^-) \int_{s/(2\hat{q}\gamma)^2}^{(2\hat{q}\gamma)^2/s} \frac{dx}{8x} n\left(\sqrt{\frac{sx}{4}}\right) n\left(\sqrt{\frac{s}{4x}}\right). \quad (9)$$

When $\hat{s}_{\min} \gg 4m_\mu^2$, which is valid for the experiments considered in Section 4, a simplified formula for the Breit-Wheeler cross section can be used:

$$\sigma(\gamma\gamma \rightarrow \mu^+\mu^-) \approx \frac{4\pi\alpha^2}{s} \left(\ln \frac{s}{m_\mu^2} - 1 \right) \text{ for } s \gg 4m_\mu^2. \quad (10)$$

In this case

$$\sigma_{\text{fid.}}^{(\hat{s})}(pp(\gamma\gamma) \rightarrow pp\mu^+\mu^-) = \frac{64\alpha^4}{3\pi} \int_{\hat{s}_{\min}}^{\hat{s}_{\max}} \frac{ds}{s^2} \left(\ln \frac{s}{m_\mu^2} - 1 \right) \ln^3 \frac{2\hat{q}\gamma}{\sqrt{s}}. \quad (11)$$

According to Eq. (6.27b) from [28], the inaccuracy of this formula originating from virtuality of the photons equals

$$\eta \sim \left(\frac{\hat{q}^2}{\sqrt{s_{\min}} m_\mu} \right)^2 \left(\ln \frac{4E^2}{s_{\min}} \right)^{-1}, \quad (12)$$

where E is the energy of the colliding particles. The accuracy is very high for muon-antimuon pair production, but it is considerably worse in the case of electron-positron pair production.

3.2 Cut on the muon transverse momentum

To apply the cut on muon transverse momentum $p_T > \hat{p}_T$, an expression for the differential cross section of the $\gamma\gamma \rightarrow \mu^+\mu^-$ reaction with respect to p_T should be substituted into (9) [34, Eq. (88.4)]:

$$d\sigma(\gamma\gamma \rightarrow \mu^+\mu^-) = \frac{2\pi\alpha^2}{s^2} \left(\frac{s+t}{t} + \frac{t}{s+t} \right) dt = \frac{8\pi\alpha^2}{sp_T} \frac{1 - 2p_T^2/s}{\sqrt{1 - 4p_T^2/s}} dp_T, \quad (13)$$

where t is the Mandelstam variable, $t = -s/2 \pm s/2 \cdot \sqrt{1 - 4p_T^2/s}$, and muons are assumed to be ultrarelativistic. The resulting expression is

$$\sigma_{\text{fid.}}^{(\hat{s}, \hat{p}_T)}(pp(\gamma\gamma) \rightarrow pp\mu^+\mu^-) = \int_{\hat{s}_{\min}}^{\hat{s}_{\max}} ds \int_{\hat{p}_T}^{\sqrt{s}/2} dp_T \frac{d\sigma(\gamma\gamma \rightarrow \mu^+\mu^-)}{dp_T} \int_{s/(2\hat{q}\gamma)^2}^{(2\hat{q}\gamma)^2/s} \frac{dx}{8x} n\left(\sqrt{\frac{sx}{4}}\right) n\left(\sqrt{\frac{s}{4x}}\right) \quad (14)$$

$$= \frac{64\alpha^4}{3\pi} \int_{\hat{s}_{\min}}^{\hat{s}_{\max}} \frac{ds}{s^2} \ln^3 \frac{2\hat{q}\gamma}{\sqrt{s}} \left(\ln \frac{1 + \sqrt{1 - 4\hat{p}_T^2/s}}{1 - \sqrt{1 - 4\hat{p}_T^2/s}} - \sqrt{1 - \frac{4\hat{p}_T^2}{s}} \right). \quad (15)$$

3.3 Cut on the muon pseudorapidity

Pseudorapidity is defined as $\eta = -\ln \tan(\theta/2)$, where θ is the angle between the momentum of the muon and the beam axis. Experimental cuts on pseudorapidity are related to the detector geometry. The muon spectrometer of the ATLAS experiment is unable to detect muons with $\theta \lesssim 10^\circ$ or $\theta \gtrsim 170^\circ$, hence the pseudorapidity cut $|\eta| < 2.4$.

For a given value of the muon pair invariant mass s , muon pseudorapidities are determined by the ratio of photon energies x . For $x = 1$ and for cuts on p_T and s implemented in Ref. [30] (see Table 1), $\sin \theta = 2p_T/\sqrt{s}$ is always larger than $2/7$. Thus $17^\circ \lesssim \theta \lesssim 163^\circ$, and the cut on η does not reduce the number of detected muon pairs. However, for $x \ll 1$ or $x \gg 1$ muons propagate in the direction of the proton beam and escape the detector. Thus, a cut on pseudorapidity can be naturally transformed into a cut on x :

$$|\eta| < \hat{\eta} \Rightarrow 1/\hat{x} < x < \hat{x}, \quad (16)$$

where

$$\hat{x} = e^{2\hat{\eta}} \cdot \frac{1 - \sqrt{1 - 4p_T^2/s}}{1 + \sqrt{1 - 4p_T^2/s}} \quad (17)$$

(see Appendix B for derivation). In this case the expression for the fiducial cross section is

$$\sigma_{\text{fid}}^{(\hat{s}, \hat{p}_T, \hat{\eta})}(pp(\gamma\gamma) \rightarrow pp\mu^+\mu^-) = \int_{\hat{s}_{\text{min}}}^{\hat{s}_{\text{max}}} ds \int_{\hat{p}_T}^{\sqrt{s}/2} dp_T \frac{d\sigma(\gamma\gamma \rightarrow \mu^+\mu^-)}{dp_T} \int_{1/\hat{x}}^{\hat{x}} \frac{dx}{8x} n\left(\sqrt{\frac{sx}{4}}\right) n\left(\sqrt{\frac{s}{4x}}\right) \quad (18)$$

$$= \frac{4\alpha^4}{\pi} \int_{\hat{s}_{\text{min}}}^{\hat{s}_{\text{max}}} \frac{ds}{s^2} \int_{\hat{p}_T}^{\sqrt{s}/2} \frac{dp_T}{p_T} \frac{1 - 2p_T^2/s}{\sqrt{1 - 4p_T^2/s}} \int_{1/\hat{x}}^{\hat{x}} \frac{dx}{x} \ln \frac{(2\hat{q}\gamma)^2}{sx} \ln \left(\frac{(2\hat{q}\gamma)^2}{s} \cdot x \right). \quad (19)$$

4 Comparison with the experimental data

4.1 Muon pair production in proton-proton collisions

The ATLAS collaboration has measured the fiducial cross section of the $pp \rightarrow pp\mu^+\mu^-$ reaction at collision energy equal to 13 TeV ($\gamma = 6.93 \cdot 10^3$) with integrated luminosity 3.2 fb^{-1} [30]. The experimental cuts are described in Table 1. The experimental result is

$$\sigma_{\text{fid.}}^{(\text{exp.})}(pp \rightarrow pp\mu^+\mu^-) = 3.12 \pm 0.07 \text{ (stat.)} \pm 0.10 \text{ (syst.) pb.} \quad (20)$$

Results of successive application of cuts are presented in Table 2. The fiducial cross section is found to be

$$\sigma_{\text{fid.}}^{(\hat{s}, \hat{p}_T, \hat{\eta})}(pp(\gamma\gamma) \rightarrow pp\mu^+\mu^-) = 3.35 \text{ pb,} \quad (21)$$

and it is in agreement with the experimental value (20). Fig. 4 compares fiducial cross sections for several bins of muon pair invariant masses with the experimental data provided in Table 3 of Ref. [30].³ The authors of Ref. [30] compare their result with theoretical predictions obtained with the help of Monte Carlo method: the SuperCHIC [29] program gives

$$\sigma_{\text{fid.}}^{[29, 30]} = 3.45 \pm 0.05 \text{ pb;} \quad (22)$$

EPA prediction corrected for the survival factor [35] (see the discussion in Appendix C) gives

$$\sigma_{\text{fid.}}^{[30, 35]} = 3.06 \pm 0.05 \text{ pb.} \quad (23)$$

Table 1: Experimental cuts for the fiducial cross section of the $pp(\gamma\gamma) \rightarrow pp\mu^+\mu^-$ reaction measured in Ref. [30].

Muon pair invariant mass range	Muon transverse momentum	Muon pseudorapidity
$12 \text{ GeV} < \sqrt{s} < 30 \text{ GeV}$	$p_T > 6 \text{ GeV}$	$ \eta < 2.4$
$30 \text{ GeV} < \sqrt{s} < 70 \text{ GeV}$	$p_T > 10 \text{ GeV}$	

Table 2: Fiducial cross sections for the reaction $pp(\gamma\gamma) \rightarrow pp\mu^+\mu^-$ calculated with the equivalent photon spectrum (2) via Eqs. (6), (11), (15) and (19).

Cuts	Cross section, pb	
No cuts	$1.7 \cdot 10^5$	
$12 \text{ GeV} < \sqrt{s} < 30 \text{ GeV}$	54.1	59.7
$30 \text{ GeV} < \sqrt{s} < 70 \text{ GeV}$	5.66	
$12 \text{ GeV} < \sqrt{s} < 30 \text{ GeV}, p_T > 6 \text{ GeV}$	5.38	6.29
$30 \text{ GeV} < \sqrt{s} < 70 \text{ GeV}, p_T > 10 \text{ GeV}$	0.91	
$12 \text{ GeV} < \sqrt{s} < 30 \text{ GeV}, p_T > 6 \text{ GeV}, \eta < 2.4$	2.85	3.35
$30 \text{ GeV} < \sqrt{s} < 70 \text{ GeV}, p_T > 10 \text{ GeV}, \eta < 2.4$	0.50	

³ Equivalent photon spectrum (2) was used to calculate the differential cross section in Fig. 4. Taking into account dipole form factor (A.6) increases the cross section by less than 0.5% in the considered energy region. Magnetic form factor (A.3) increases the cross section by $\approx 6\%$.

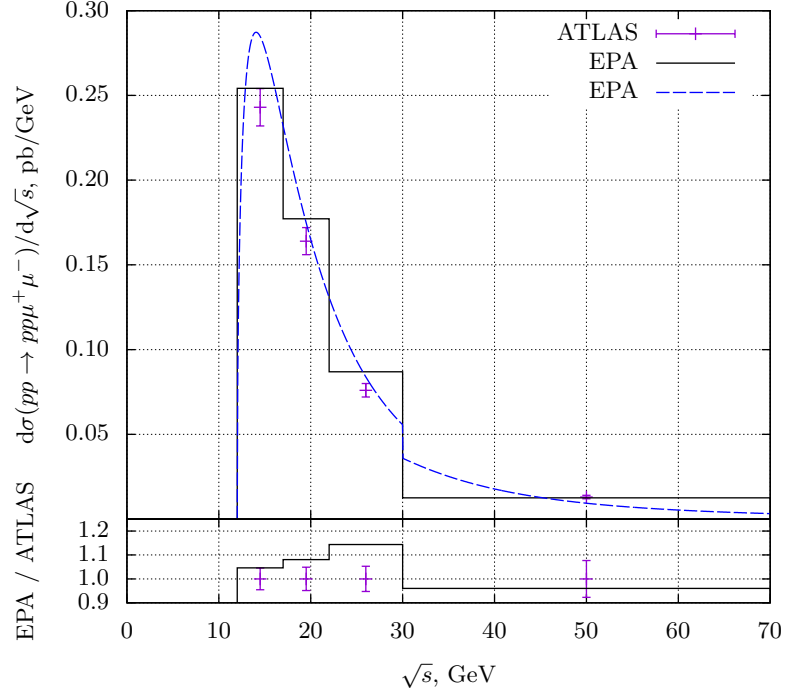


Figure 4: *Upper plot:* fiducial cross section for the $pp(\gamma\gamma) \rightarrow pp\mu^+\mu^-$ reaction at proton-proton collision energy 13 TeV with the cuts described in Table 1. Points are the experimental data presented in Table 3 of Ref. [30]. The dashed line is the differential cross section calculated with the help of (19). The histogram is the differential cross section averaged according to the bins also presented in Table 3 of Ref. [30]. *Lower plot:* ratio of the calculated cross section to the experimental points.

4.2 Muon pair production in lead-lead collisions

The ATLAS collaboration has measured the fiducial cross section of the $Pb\ Pb \rightarrow Pb\ Pb\ \mu^+\mu^-$ reaction at collision energy per nucleon pair equal to 5.02 TeV ($\gamma = 2.69 \cdot 10^3$) with integrated luminosity $515\ \mu b^{-1}$ [31]. The experimental cuts are:

- Muon pair invariant mass range: $10\ \text{GeV} < \sqrt{s} < 100\ \text{GeV}$.
- Muon transverse momentum: $p_T > 4\ \text{GeV}$.
- Muon pseudorapidity: $|\eta| < 2.4$.

The experimental result is

$$\sigma_{\text{fid.}}^{(\text{exp.})}(Pb\ Pb \rightarrow Pb\ Pb\ \mu^+\mu^-) = 32.2 \pm 0.3\ (\text{stat.})_{-3.4}^{+4.0}\ (\text{syst.})\ \mu b. \quad (24)$$

A heavy nucleus is easier to break apart than a proton. Maximum momentum transfer for a proton is $\hat{q} \approx 0.20\ \text{GeV}$ (A.8). The corresponding value for ^{208}Pb heavily depends on the nucleus form factor, but it is about an order of magnitude less. In the leading logarithmic approximation, maximum photon energy is $2\hat{q}\gamma$. For the protons with the collision energy of 13 TeV, this value is 2.8 TeV, while for the lead-lead collision considered in this section, it is about 100 GeV. Consequently, lead-lead collisions are much more sensitive to the shape of electromagnetic form factor of colliding particles.

To calculate the fiducial cross sections, Eq. (18) was used with several equivalent photon spectra $n(\omega)$ corresponding to different form factors [36, 37]. Fig. 5 compares the results with the experimental data presented in the left plot in Fig. 3 of Ref. [31].⁴ The spectrum with the form factor described by Fourier-Bessel parameters from Ref. [37] (see Table 4) and the spectrum with the monopole form factor with the parameter $\Lambda = 50\ \text{MeV}$ both describe the experimental data well. The leading logarithmic approximation with $\hat{q} = 18\ \text{MeV}$ (A.14)

⁴ The two sets of data points in the left plot in Fig. 3 of Ref. [31] are for two cuts on dimuon pair rapidity $Y_{\mu\mu}$. The cut on dimuon pair rapidity is not considered in this paper. The cut $|Y_{\mu\mu}| < 2.4$ used for the upper curve corresponds to the cut $|\eta| < 2.4$.

is accurate at low invariant masses, but at high invariant masses it underestimates the number of equivalent photons. The reason is that in this region the assumption $\omega \ll \hat{q}\gamma \approx 50$ GeV used in the derivation of Eq. (2) is not valid. The form factor described by Fourier-Bessel parameters in earlier publication [36] (see Table. 4) and its approximation with the monopole form factor with the parameter $\Lambda = 80$ MeV often used in literature [38–40] result in the fiducial cross section about 1.5 times larger than measured.

Fiducial cross section calculated with the spectrum with the form factor obtained from Fourier-Bessel parameters from Ref. [37],

$$\sigma_{\text{fid.}}^{(\hat{s}, \hat{p}_T, \hat{\eta})}(\text{Pb Pb } (\gamma\gamma) \rightarrow \text{Pb Pb } \mu^+ \mu^-) = 34.4 \text{ } \mu\text{b}, \quad (25)$$

is in agreement with the experimental value (24). Cross sections calculated with successive application of the cuts are summarized in Table 3.

The authors of Ref. [31] compare the measured result with calculations with the help of the STARLIGHT program [41]:

$$\sigma_{\text{fid.}}^{[31,41]}(\text{Pb Pb } (\gamma\gamma) \rightarrow \text{Pb Pb } \mu^+ \mu^-) = 31.64 \pm 0.04 \text{ } \mu\text{b}. \quad (26)$$

Table 3: Fiducial cross sections for the reaction $\text{Pb Pb } (\gamma\gamma) \rightarrow \text{Pb Pb } \mu^+ \mu^-$ with the nucleus form factor approximated by the monopole formula (A.11) with $\Lambda = 50$ MeV.

Cuts	Cross section, μb
No cuts	$1.92 \cdot 10^6$
$10 \text{ GeV} < \sqrt{s} < 100 \text{ GeV}$	264
also $p_T > 4 \text{ GeV}$	42.5
also $ \eta < 2.4$	34.6

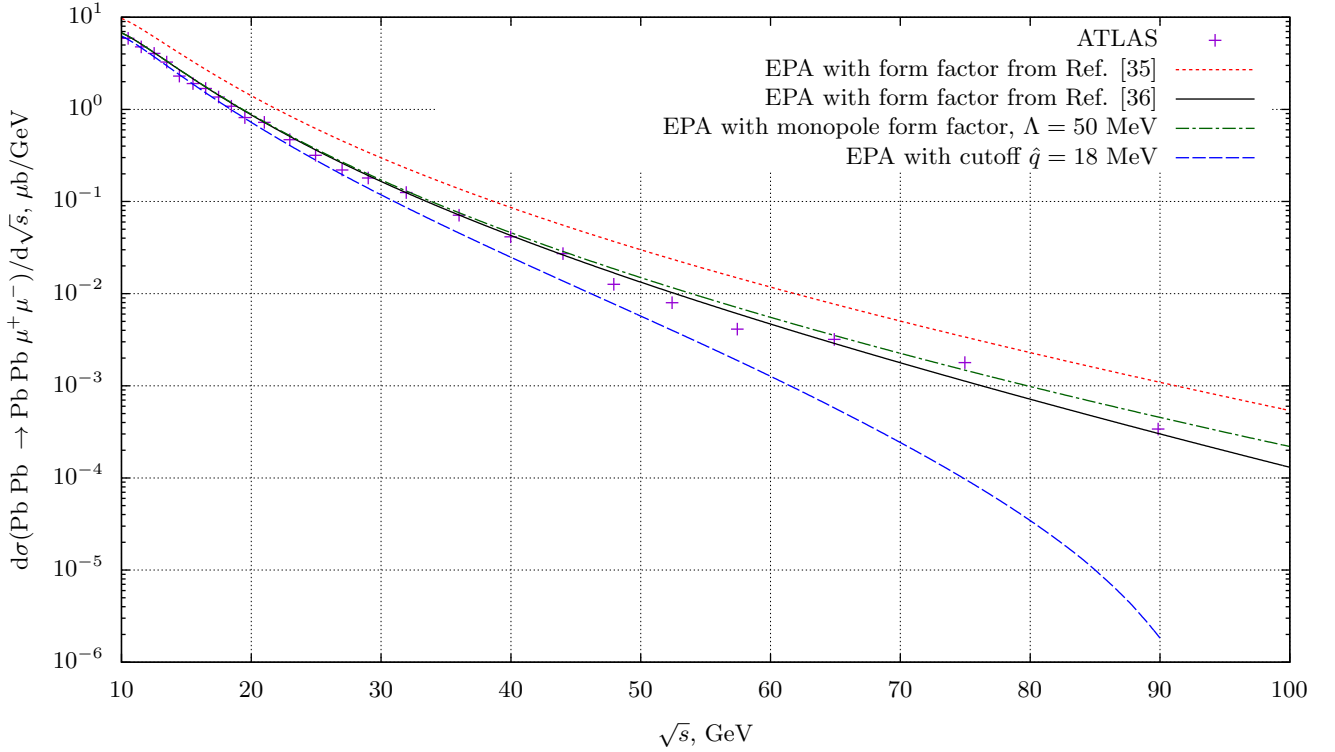


Figure 5: Fiducial cross section for the $\text{Pb Pb } (\gamma\gamma) \rightarrow \text{Pb Pb } \mu^+ \mu^-$ reaction at collision energy per nucleon pair 5.02 TeV with the experimental cuts of Ref. [31] (also described in the text). Points are experimental data from the left plot of Fig. 3 of Ref. [31] (the upper curve). The lines were calculated with the help of (18). The red dotted and black solid lines are calculated using the equivalent photon spectra with form factors from Refs. [36] and [37] correspondingly. The green dash-dotted line corresponds to the spectrum with monopole form factor with the parameter $\Lambda = 50$ MeV. For the blue dashed line the spectrum (2) was used with $\hat{q} = 18$ MeV.

5 Conclusions

The LHC can be used to search for New Physics appearing in photon-photon collisions. Photon pair invariant mass can reach $2\hat{q}\gamma \approx 2.8$ TeV in pp collisions with the energy equal to 13 TeV and ≈ 100 GeV in Pb Pb collisions with the energy per nucleon pair equal to 5.02 TeV.

The equivalent photon approximation permits analytical calculation of fiducial cross section. Leading logarithmic approximation (2) provides both accurate results and relatively simple expressions at invariant masses much less than $\hat{q}\gamma$. At higher invariant masses form factors of the colliding particles have to be taken into account.

Although experimental cuts greatly reduce the production cross section, high luminosity achieved at the LHC makes it possible to observe $\mu^+\mu^-$ pair production in ultraperipheral collisions.

We are grateful to A. N. Rozanov, discussion with whom triggered out interest to the LHC results on $\gamma\gamma$ reactions, to I. I. Tsukerman for useful comments, to H. Terazawa for drawing our attention to papers [26, 33], to I. F. Ginzburg for a very useful discussion, to S. I. Godunov for the help with checking our numerical calculations, and to V. A. Novikov for the ideas implemented in Appendix C. We were supported by the RFBR grant 16-02-00342. Work on Sections 2, 3 and Appendix C was supported by the RSF grant 19-12-00123.

A Equivalent photons momentum cutoff

Consider a charged particle at rest. Its electromagnetic field can be interpreted as a collection of virtual photons with zero energy. Let $q = (0, q_x, q_y, q_z)$ be the momentum of such a virtual photon. When the particle is boosted with the Lorentz factor $\gamma \gg 1$ along the z axis, the photon acquires energy $\omega = \sqrt{\gamma^2 - 1} q_z$ approximately equal to the photon momentum in the boost direction γq_z . The virtuality of such a photon, $-q^2 = q_x^2 + q_y^2 + q_z^2 \ll \omega^2$, so the photon can be considered real, and this is the essence of the equivalent photon approximation.

To obtain the spectrum of virtual photons $n(\omega)$ (2) of a moving particle, the distribution of virtual photons $n(\vec{q}) d^3q$ (1) has to be integrated over the photon transverse momentum $q_\perp = \sqrt{q_x^2 + q_y^2}$. This integral is logarithmically divergent at high q_\perp , and a cutoff is required. In a collision, if a proton (or a nucleus) emits a virtual photon of sufficiently high momentum, the proton breaks apart. Thus, a natural estimation for the cutoff value \hat{q} would be the inverse radius of the proton or the QCD scale Λ_{QCD} which is in the range of 200–300 MeV [42, Section 9]. In the case of e^+e^- pair production, $\hat{q} = m_e$ since contribution of the $q_\perp > m_e$ domain is power suppressed.

A more rigorous approach to obtain the cutoff value \hat{q} for proton is to consider the proton form factor. The Dirac form factor is [43]

$$F_1(q^2) = \frac{G_E(q^2) + \tau G_M(q^2)}{1 + \tau}, \quad (\text{A.1})$$

where $\tau = -q^2/4m_p^2$,

$$G_E(q^2) = \frac{1}{(1 - q^2/\Lambda^2)^2} \quad (\text{A.2})$$

is the electric form factor,

$$G_M(q^2) = \frac{\mu_p}{(1 - q^2/\Lambda^2)^2} \quad (\text{A.3})$$

is the magnetic form factor, $\mu_p = 2.79$ is the proton magnetic moment and $\Lambda^2 = 0.71 \text{ GeV}^2$. Eq. (A.1) can be rearranged as follows

$$F_1(q^2) = G_D(q^2) \left[1 + \frac{(\mu_p - 1)\tau}{1 + \tau} \right], \quad (\text{A.4})$$

where $G_D(q^2) \equiv G_E(q^2)$ is the dipole form factor. Since $-q^2 \approx q_\perp^2$ cannot be much larger than Λ_{QCD}^2 , $\tau \ll 1$ and the contribution from the magnetic form factor can be neglected. Deriving the equivalent photon momentum distribution (1) according to [34, §99] and taking into account the form factor results in

$$n_{\text{dipole}}(\vec{q}) d^3q = \frac{\alpha}{\pi^2} \frac{\vec{q}_\perp^2}{\omega q^4} \left(1 - \frac{q^2}{\Lambda^2} \right)^{-4} d^3q = \frac{\alpha}{\pi^2 \omega} \frac{\vec{q}_\perp^2}{(\omega^2/\gamma^2 + q_\perp^2)^2} \left(1 + \frac{1}{\Lambda^2} \left(\frac{\omega^2}{\gamma^2} + q_\perp^2 \right) \right)^{-4} d^3q. \quad (\text{A.5})$$

The equivalent photon spectrum

$$n_{\text{dipole}}(\omega) d\omega = 2\pi \int_0^\infty n_{\text{dipole}}(\vec{q}) q_\perp dq_\perp d\omega = \frac{\alpha}{\pi} \left[(4a + 1) \ln \left(1 + \frac{1}{a} \right) - \frac{24a^2 + 42a + 17}{6(a + 1)^2} \right] \frac{d\omega}{\omega}, \quad (\text{A.6})$$

where $a = (\omega/\Lambda\gamma)^2$. This function monotonically decreases with ω . In the lower energy limit $\omega \ll \Lambda\gamma$, where most of the photons reside,

$$n_{\text{dipole}}(\omega)d\omega \xrightarrow{a \rightarrow 0} \frac{\alpha}{\pi} \left[2 \ln \frac{\Lambda\gamma}{\omega} - \frac{17}{6} \right] \frac{d\omega}{\omega}. \quad (\text{A.7})$$

Comparing this expression with Eq. (2) for $Z = 1$, we get

$$\hat{q} = \Lambda e^{-\frac{17}{12}} \approx 0.20 \text{ GeV}, \quad (\text{A.8})$$

which is in a perfect agreement with the previous assumption that $\hat{q} \approx \Lambda_{\text{QCD}}$.

Heavy nucleus form factor is more involved. The most accurate description of the ^{208}Pb form factor appears to be the Fourier transform of Bessel decomposition of the nucleus charge density distribution [44]:

$$\rho(r) = \begin{cases} \sum_{n=1}^N a_n j_0(n\pi r/R) & \text{for } r \leq R, \\ 0 & \text{for } r \geq R, \end{cases} \quad (\text{A.9})$$

where $j_0(x) = \sin(x)/x$ is the Bessel function of order zero, and the values of a_n and R are provided in Table 4. The corresponding form factor is

$$F_{\text{Fourier-Bessel}}(q^2) = \frac{\int \rho(r) e^{i\vec{q}\vec{r}} d^3r}{\int \rho(r) d^3r} = \frac{\sin qR}{qR} \cdot \frac{\sum_{n=1}^N \frac{(-1)^n a_n}{n^2 \pi^2 - q^2 R^2}}{\sum_{n=1}^N \frac{(-1)^n a_n}{n^2 \pi^2}}. \quad (\text{A.10})$$

Heavy nucleus form factor is often approximated by a monopole formula:

$$F_{\text{monopole}}(q^2) \approx \frac{1}{1 - q^2/\Lambda^2}. \quad (\text{A.11})$$

The corresponding equivalent photon spectrum is

$$n_{\text{monopole}}(\omega)d\omega = \frac{Z^2\alpha}{\pi} \left[(2a+1) \ln \left(1 + \frac{1}{a} \right) - 2 \right] \frac{d\omega}{\omega}. \quad (\text{A.12})$$

In the low energy limit

$$n_{\text{monopole}}(\omega)d\omega \xrightarrow{a \rightarrow 0} \frac{Z^2\alpha}{\pi} \left[2 \ln \frac{\Lambda\gamma}{\omega} - 2 \right] \frac{d\omega}{\omega}, \quad (\text{A.13})$$

Table 4: Parameters of the Fourier-Bessel decomposition of ^{208}Pb form-factor (A.10).

Ref.	[36] ^a	[37]
$R, \text{ fm}$	11.0	12.5
a_1	0.62732×10^{-1}	1.4396×10^0
a_2	0.38542×10^{-1}	-4.1850×10^{-1}
a_3	-0.55105×10^{-1}	-9.1763×10^{-2}
a_4	-0.26990×10^{-2}	6.8006×10^{-2}
a_5	0.31016×10^{-1}	2.6476×10^{-2}
a_6	-0.99486×10^{-2}	-1.5307×10^{-2}
a_7	-0.93012×10^{-2}	-7.1246×10^{-3}
a_8	0.76653×10^{-2}	2.7987×10^{-3}
a_9	0.20885×10^{-2}	2.3767×10^{-3}
a_{10}	-0.17840×10^{-2}	-1.0125×10^{-3}
a_{11}	0.74876×10^{-4}	-2.5836×10^{-4}
a_{12}	0.32278×10^{-3}	6.4297×10^{-5}
a_{13}	-0.11353×10^{-3}	6.5528×10^{-5}
a_{14}		1.4523×10^{-5}
a_{15}		-1.4430×10^{-5}

^a There are two sets of parameters in Ref. [36]. The corresponding form factors almost coincide.

so

$$\hat{q} = \Lambda e^{-1}. \quad (\text{A.14})$$

For $\Lambda = 80$ MeV that was used in [38–40], $\hat{q} \approx 30$ MeV. However, this value of Λ apparently approximates outdated data. Fig. 6 compares monopole form factor with $\Lambda = 80$ MeV to form factors calculated through Fourier-Bessel decomposition with the parameters that were fit to the experimental data available in 1987 [36] and in 1995 [37] (see Table 4). Monopole form factor with $\Lambda = 50$ MeV ($\hat{q} \approx 18$ MeV) used in Section 4.2 is presented as well for the reference.

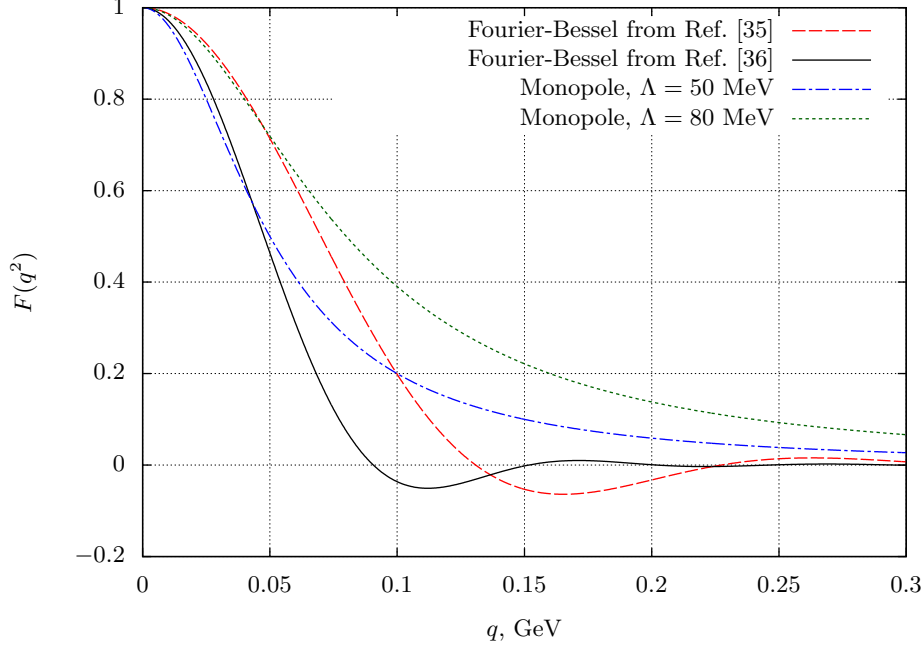


Figure 6: ^{208}Pb form factors available in the literature and their approximations. The solid black and the dashed red lines are form factors described through Fourier-Bessel decomposition (A.10). Parameters a_n and R for the former were taken from Ref. [37], for the latter—from Ref. [36]. The blue dash-dotted and the green dotted lines are monopole form-factors (A.11) with the parameters $\Lambda = 50$ MeV and $\Lambda = 80$ MeV correspondingly.

B Pseudorapidity cut

In order to take the pseudorapidity cut into account, the photon energy ratio $x = \omega_1/\omega_2$ has to be expressed through the muon pair invariant mass s , muon transverse momentum p_T , and muon pseudorapidity η . A collision of two photons with the energies ω_1 and ω_2 is shown in Fig. 7. μ^+ with momentum p^+ and μ^- with momentum p^- are produced in this collision. In the following $p_T \gg m_\mu$ is assumed, and the muon mass m_μ is neglected; this is valid for the experiments considered in this paper.

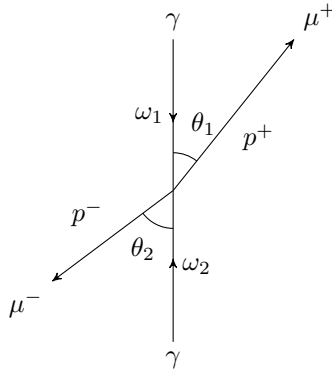


Figure 7: $\gamma\gamma \rightarrow \mu^+\mu^-$ reaction.

From the conservation of energy and momenta

$$\begin{cases} p_T^+ = -p_T^- \equiv p_T, \\ \omega_1 + \omega_2 = \sqrt{p_T^2 + p_{\parallel}^{+2}} + \sqrt{p_T^2 + p_{\parallel}^{-2}}, \\ \omega_1 - \omega_2 = p_{\parallel}^- - p_{\parallel}^+. \end{cases} \quad (\text{B.1})$$

The last two equations can be expressed through the transverse momentum p_T and the scattering angles θ_1 and θ_2 :

$$\begin{cases} \frac{p_T}{\sin \theta_1} + \frac{p_T}{\sin \theta_2} = \omega_1 + \omega_2, \\ \frac{p_T}{\tan \theta_1} - \frac{p_T}{\tan \theta_2} = \omega_1 - \omega_2. \end{cases} \quad (\text{B.2})$$

The scattering angles are related to pseudorapidity through equation

$$\eta_i = -\ln \tan(\theta_i/2), \quad i = 1, 2, \quad (\text{B.3})$$

so

$$\begin{cases} \cosh \eta_1 + \cosh \eta_2 = \frac{\omega_1 + \omega_2}{p_T}, \\ \sinh \eta_1 - \sinh \eta_2 = \frac{\omega_1 - \omega_2}{p_T}. \end{cases} \quad (\text{B.4})$$

Elimination of η_2 results in the equation

$$e^{2\eta_1} - \frac{2\omega_1}{p_T} e^{\eta_1} + \frac{\omega_1}{\omega_2} = 0. \quad (\text{B.5})$$

Substitution of $\omega_1 = \sqrt{sx/4}$, $\omega_2 = \sqrt{s/4x}$ leads to

$$e^{2\eta_1} - \frac{\sqrt{sx}}{p_T} e^{\eta_1} + x = 0. \quad (\text{B.6})$$

The solution of this equation with respect to x is

$$x = e^{2\eta_1} \cdot \frac{(1 \pm \sqrt{1 - 4p_T^2/s})^2}{4p_T^2/s} = e^{2\eta_1} \cdot \frac{1 \pm \sqrt{1 - 4p_T^2/s}}{1 \mp \sqrt{1 - 4p_T^2/s}}. \quad (\text{B.7})$$

With η_1 varying from $-\hat{\eta}$ to $\hat{\eta}$, x varies in the following intervals:

$$\begin{cases} e^{-2\hat{\eta}} \cdot \frac{1 + \sqrt{1 - 4p_T^2/s}}{1 - \sqrt{1 - 4p_T^2/s}} < x < e^{2\hat{\eta}} \cdot \frac{1 + \sqrt{1 - 4p_T^2/s}}{1 - \sqrt{1 - 4p_T^2/s}}, \\ e^{-2\hat{\eta}} \cdot \frac{1 - \sqrt{1 - 4p_T^2/s}}{1 + \sqrt{1 - 4p_T^2/s}} < x < e^{2\hat{\eta}} \cdot \frac{1 - \sqrt{1 - 4p_T^2/s}}{1 + \sqrt{1 - 4p_T^2/s}}. \end{cases} \quad (\text{B.8})$$

To satisfy both $\eta_1 < |\hat{\eta}|$ and $\eta_2 < |\hat{\eta}|$, the intersection of these intervals has to be selected. Hence

$$1/\hat{x} < x < \hat{x} \text{ where } \hat{x} = e^{2\hat{\eta}} \cdot \frac{1 - \sqrt{1 - 4p_T^2/s}}{1 + \sqrt{1 - 4p_T^2/s}}. \quad (\text{B.9})$$

When applying these inequalities to setup the integration domain for the equivalent photon approximation, a check that the photon energy does not exceed the cutoff energy $\hat{q}\gamma$ is required:

$$\hat{x} < \frac{(2\hat{q}\gamma)^2}{s}. \quad (\text{B.10})$$

This is always true for the reaction $pp(\gamma\gamma) \rightarrow pp\mu^+\mu^-$ with the cuts implemented in [30]. However, in the case of Pb Pb $(\gamma\gamma) \rightarrow \text{Pb Pb } \mu^+\mu^-$ reaction with the cuts used in [31], this inequality provides an additional cut on x which should be accounted for when calculating the fiducial cross section with cutoff \hat{q} .

C Survival factor

It is well known that the distribution of equivalent photons given by (2) can be obtained from the classical consideration of the electromagnetic field of an ultrarelativistic charged particle. The solution of Maxwell equations for the electromagnetic field induced by an ultrarelativistic charged particle moving in the direction of z axis is [45, Eq. (33.2.3)]

$$\begin{aligned}\vec{E}_\perp(\vec{r}, t) &= -\frac{iZe\gamma}{(2\pi)^3} \int \frac{\vec{q}_\perp}{\vec{q}^2} e^{i\vec{q}_\perp \cdot \vec{r} + i\gamma q_z(z-vt)} d^3q, \\ \vec{H}(\vec{r}, t) &= \vec{v} \times \vec{E}(\vec{r}, t),\end{aligned}\tag{C.1}$$

where $\vec{E}(\vec{r}, t)$ and $\vec{H}(\vec{r}, t)$ are electric and magnetic fields at point \vec{r} at the moment t , \vec{E}_\perp is the component of \vec{E} transverse to the z axis, v is the particle velocity, and \vec{q} is the Fourier transformation parameter.

Electric field in the z direction is not enhanced by the Lorentz factor γ . Thus for $\gamma \gg 1$, $E_\perp \gg |E_z|$ and the electric field is practically transversal, just as it should be in the case of real photons. In this way equation (C.1) gives expansion of electromagnetic fields in terms of monochromatic plane waves moving in the z direction and having frequencies $\omega = v\gamma q_z \approx \gamma q_z$.

Total flux of the electromagnetic energy flowing in the z direction is given by the Poynting vector component:

$$\Pi_z = \int d^2b \int_{-\infty}^{\infty} dt [\vec{E} \times \vec{H}]_z,\tag{C.2}$$

where $\vec{b} \equiv \vec{r}_\perp$ is the impact parameter for point \vec{r} . Π_z is equal to the total energy of equivalent photons:

$$\Pi_z = \int_0^\infty \omega n(\omega) d\omega.\tag{C.3}$$

Substitution of expansion (C.1) into Eq. (C.2) results in:

$$\begin{aligned}\Pi_z &= \int d^2b \int dt (E_x^2 + E_y^2) = \frac{Z^2 e^2 \gamma^2}{(2\pi)^6} \int d^2b dt d^3q d^3q' \frac{-q_x q'_x - q_y q'_y}{\vec{q}^2 \vec{q}'^2} \\ &\quad \times \exp[ix(q_x + q'_x) + iy(q_y + q'_y) + i\gamma(z-vt)(q_z + q'_z)] F(\vec{q}^2) F(\vec{q}'^2),\end{aligned}\tag{C.4}$$

where the form factor of the charged particle is taken into account. Integration of (C.4) over d^2b and dt results in three delta functions which then remove the integral over d^3q' . The final expression for the z component of the Poynting vector is

$$\Pi_z = \frac{Z^2 \alpha \gamma}{2\pi^2} \int \frac{\vec{q}_\perp^2 F^2(\vec{q}_\perp^2 + \omega^2/\gamma^2)}{(\vec{q}_\perp^2 + \omega^2/\gamma^2)^2} d^3q.\tag{C.5}$$

Changing the integration variable q_z to ω and comparing the result with (C.3), we obtain:

$$n(\omega) d\omega = \frac{Z^2 \alpha}{\pi^2} \int \frac{\vec{q}_\perp^2 F^2(\vec{q}_\perp^2 + \omega^2/\gamma^2)}{(\vec{q}_\perp^2 + \omega^2/\gamma^2)^2} d^2q_\perp \frac{d\omega}{\omega},\tag{C.6}$$

where the extra factor of 2 comes from the fact that when q_z varies from $-\infty$ to ∞ , ω covers the region $[0; \infty)$ twice. The difference between this expression and (2) is that here the form factor is taken into account.

In order to introduce the notion of survival factor, the integration over d^2b in (C.4) should be postponed until the end. Let us define $n(b, \omega)$ through the following equation:

$$n(\omega) = \int n(b, \omega) d^2b.\tag{C.7}$$

Integrating (C.4) over dt and performing integration over dq'_z with the help of the delta function, we obtain:

$$n(b, \omega) = \frac{Z^2 \alpha}{4\pi^4 \omega} \int dq_\perp d\theta \frac{q_\perp F(q_\perp^2 + \omega^2/\gamma^2)}{q_\perp^2 + \omega^2/\gamma^2} \int dq'_\perp d\theta' \frac{q'_\perp F(q'_\perp^2 + \omega^2/\gamma^2)}{q'^2_\perp + \omega^2/\gamma^2} (-q_\perp q'_\perp) \cos(\theta - \theta') e^{ibq_\perp \cos \theta} e^{ibq'_\perp \cos \theta'},\tag{C.8}$$

where θ is the angle between \vec{q}_\perp and \vec{b} , and θ' is the angle between \vec{q}'_\perp and \vec{b} .

The next step is to use the integral representation of the Bessel function:

$$\begin{aligned} \int_0^{2\pi} \cos \theta e^{ia \cos \theta} d\theta &= 2i\pi J_1(a), \\ \int_0^{2\pi} \sin \theta e^{ia \cos \theta} d\theta &= 0, \end{aligned} \quad (\text{C.9})$$

and the expansion $\cos(\theta - \theta') = \cos \theta \cos \theta' + \sin \theta \sin \theta'$:

$$n(b, \omega) = \frac{Z^2 \alpha}{\pi^2 \omega} \left[\int dq_\perp q_\perp^2 \frac{F(q_\perp^2 + \omega^2/\gamma^2)}{q_\perp^2 + \omega^2/\gamma^2} J_1(bq_\perp) \right]^2. \quad (\text{C.10})$$

With the help of the identity

$$\int_0^\infty J_1(ax) J_1(bx) x dx = \frac{1}{a} \delta(a - b), \quad (\text{C.11})$$

transition from (C.10) through (C.7) to (C.6) is straightforward.

For a standalone ultrarelativistic charged particle, its finite transversal size is taken into account by the form factor F which tends to 0 for high transverse photon momentum q_\perp . However, when an ultraperipheral collision of two ultrarelativistic charged particles is considered, one should factor in the probability that this collision is indeed ultraperipheral, i.e., that the particles remain intact after the collision. If the particles are modeled as black disks, then the necessary requirement is that their impact parameter $b = |\vec{b}_2 - \vec{b}_1|$ is greater than the sum of their radii. More elaborate model of the particles interaction can be described through the function $P(b)$ which is the probability for the particles to remain intact after passing each other at distance b . Then the cross section for production of a system X in an ultraperipheral collision is

$$\sigma(NN \rightarrow NNX) = \int_0^\infty d\omega_1 \int_0^\infty d\omega_2 \sigma(\gamma\gamma \rightarrow X) \int d^2b_1 \int d^2b_2 n(b_1, \omega_1) n(b_2, \omega_2) P(|\vec{b}_2 - \vec{b}_1|), \quad (\text{C.12})$$

where N is the colliding particle, and $\sigma(\gamma\gamma \rightarrow X)$ is the cross section for the production of X through the photon fusion. For point-like particles $P(b) = 1$, and

$$\sigma(NN \rightarrow NNX) = \int_0^\infty d\omega_1 \int_0^\infty d\omega_2 \sigma(\gamma\gamma \rightarrow X) n(\omega_1) n(\omega_2). \quad (\text{C.13})$$

(The difference between (C.13) and (3) is that in (C.13) the integration is cut off at high ω_i through the form factors, while in (3) it is done explicitly through the \hat{q} parameter.) In [35], survival factor is defined as

$$S_{\gamma\gamma}^2 = \frac{\int_{b_1 > R} \int_{b_2 > R} n(b_1, \omega_1) n(b_2, \omega_2) P(|\vec{b}_2 - \vec{b}_1|) d^2b_1 d^2b_2}{\int_{b_1 > 0} \int_{b_2 > 0} n(b_1, \omega_1) n(b_2, \omega_2) d^2b_1 d^2b_2}, \quad (\text{C.14})$$

where R is the radius of the colliding particle. The form factor of the particle $F(\vec{q}_\perp^2 + \omega^2/\gamma^2)$ cuts off the integration in Eq. (C.10) at large q_\perp or, equivalently, at small b . Consequently the integration in the nominator should not explicitly cut off the regions $b_1, b_2 < R$. Thus the formula for the survival factor we suggest is

$$S_{\gamma\gamma}^2 = \frac{\int_{b_1 > 0} \int_{b_2 > 0} n(b_1, \omega_1) n(b_2, \omega_2) P(|\vec{b}_2 - \vec{b}_1|) d^2b_1 d^2b_2}{n(\omega_1) n(\omega_2)}. \quad (\text{C.15})$$

References

- [1] L. D. Landau, E. M. Lifshitz. Production of electrons and positrons by a collision of two particles. Phys.Zs.Sowjet 6, 244 (1934).
- [2] C. A. Bertulani, G. Baur. Electromagnetic processes in relativistic heavy ion collisions. Phys.Rept. 163, 299 (1988).

- [3] G. Baur, K. Hencken, D. Trautmann, S. Sadovsky, Yu. Kharlov. Coherent gamma-gamma and gamma-A interactions in very peripheral collisions at relativistic ion colliders. Phys.Rept. 364, 359 (2001). [arXiv:hep-ph/0112211](#)
- [4] G. Baur. Physics opportunities in ultraperipheral heavy ion collisions at LHC. Proc. of Workshop on electromagnetic problems of fundamental physics, Oct. 16–21, 2001, Erice, Italy. [arXiv:hep-ph/0112239](#)
- [5] G. Baur, C. A. Bertulani, M. Chiu, I. F. Ginzburg *et. al.* Hot topics in ultra-peripheral collisions. [arXiv:hep-ex/0201034](#)
- [6] L. Frankfurt, M. Strikman, M. Zhalov. Coherent photoproduction from nuclei. Acta Phys.Polon. B34, 3215 (2003). [arXiv:hep-ph/0304301](#)
- [7] C. A. Bertulani, S. R. Klein, J. Nystrand. Physics of ultra-peripheral nuclear collisions. Ann.Rev.Nucl.Part.Sci. 55, 271 (2005). [arXiv:nucl-ex/0502005](#)
- [8] J. Nystrand. Ultra-peripheral collisions of heavy ions at RHIC and the LHC. Nucl.Phys. A787, 29 (2007). [arXiv:hep-ph/0611042](#)
- [9] A. J. Baltz, G. Baur, D. d’Enterria, L. Frankfurt *et. al.* The physics of ultraperipheral collisions at the LHC. Phys.Rept. 458, 1 (2008). [arXiv:0706.3356](#)
- [10] G. Baur. Coherent photon-photon interactions in very peripheral relativistic heavy ion collisions. Eur.Phys.J. D55, 265 (2009). [arXiv:0810.1400](#)
- [11] M. Klusek-Gawenda, A. Szczurek. Exclusive production of large invariant mass pion pairs in ultraperipheral ultrarelativistic heavy ion collisions. Phys.Lett. B700, 322 (2011). [arXiv:1104.0571](#)
- [12] A. Szczurek. Peripheral, ultrarelativistic production of particles in heavy ion collisions. Acta Phys.Polon. B45, 1597 (2014). [arXiv:1404.0896](#)
- [13] M. Klusek-Gawenda, P. Lebiedowicz, A. Szczurek. Light-by-light scattering in ultraperipheral PbPb collisions at the Large Hadron Collider. Phys.Rev. C93, 044907 (2016). [arXiv:1601.07001](#)
- [14] M. Klusek-Gawenda, A. Szczurek. Double scattering production of two positron-electron pairs in ultraperipheral heavy-ion collisions. Phys.Lett. B763, 416 (2016). [arXiv:1607.05095](#)
- [15] M. B. Gay Ducati, F. Kopp, M. V. T. Machado, S. Martins. Photoproduction of Upsilon states in ultraperipheral collisions at the CERN Large Hadron Collider with the color dipole approach. Phys.Rev. D94, 094023 (2016). [arXiv:1610.06647](#)
- [16] M. Klusek-Gawenda, P. Lebiedowicz, O. Nachtmann, A. Szczurek. From the $\gamma\gamma \rightarrow p\bar{p}$ reaction to the production of $p\bar{p}$ pairs in ultraperipheral ultrarelativistic heavy-ion collisions at the LHC. Phys.Rev. D96, 094029 (2017). [arXiv:1708.09836](#)
- [17] The ATLAS collaboration. Technical Design Report for the ATLAS Forward Proton Detector. CERN-LHCC-2015-009, ATLAS-TDR-024-2015 (2015).
- [18] The CMS and TOTEM collaborations. CMS-TOTEM Precision Proton Spectrometer. CERN-LHCC-2014-021, TOTEM-TDR-003 (2014).
- [19] CMS Luminosity—Public Results.
<https://twiki.cern.ch/twiki/bin/view/CMSPublic/LumiPublicResults>
- [20] ATLAS Luminosity—Public Results.
<https://twiki.cern.ch/twiki/bin/view/AtlasPublic/LuminosityPublicResultsRun2>
- [21] J. M. Jowett, M. Schaumann, R. Alemany, *et. al.* The 2015 heavy-ion run of the LHC. 7th International Particle Accelerator Conference, Busan, Korea, 08 May 2018 – 13 May 2018
- [22] E. Fermi. Über die Theorie des Stoßes zwischen Atomen und elektrisch geladenen Teilchen. Z.Physik 29, 315 (1924).
- [23] C. F. V. Weizsäcker. Ausstrahlung bei Stößen sehr schneller Elektronen. Z.Physik 88, 612 (1934).
- [24] E. J. Williams. Correlation of certain collision problems with radiation theory. Kgl. Danske Vidensk. Selskab. Mat.-Fiz. Medd. 13, 4 (1935).

- [25] V. E. Balakin, V. M. Budnev, I. F. Ginzburg. Feasibility of an experiment in which hadrons are produced by two protons from threshold to extremely large energies. JETP Lett. 11, 388 (1970).
- [26] H. Terazawa, Two-photon processes for particle production at high energies. Rev.Mod.Phys. 4, 615 (1973).
- [27] V. M. Budnev, I. F. Ginzburg, G. V. Meledin, V. G. Serbo. The two-photon particle production and the equivalent photon approximation. Particles & Nuclei 4, 239 (1973) [in Russian].
- [28] V. M. Budnev, I. F. Ginzburg, G. V. Meledin, V. G. Serbo. The two-photon particle production mechanism. Physical problems. Applications. Equivalent photon approximation. Phys.Rep. 15, 181 (1975)
- [29] L. A. Harland-Lang, V. A. Khoze, M. G. Ryskin. Exclusive physics at the LHC with SuperChic 2. Eur.Phys.J. C76, 9 (2016). [arXiv:1508.02718](#)
- [30] The ATLAS Collaboration. Measurement of the exclusive $\gamma\gamma \rightarrow \mu^+\mu^-$ process in proton-proton collisions at $\sqrt{s} = 13$ TeV with the ATLAS detector. Phys.Lett. B 777, 303 (2018). [arXiv:1708.04053](#)
- [31] The ATLAS Collaboration. Measurement of high-mass dimuon pairs in ultra-peripheral lead-lead collisions at $\sqrt{s_{NN}} = 5.02$ TeV with the ATLAS detector at the LHC. ATLAS-CONF-2016-025 (2016).
- [32] G. Breit, J. A. Wheeler. Collision of two light quanta. Phys.Rev. 46, 1087 (1934).
- [33] S. J. Brodsky, T. Kinoshita, H. Terazawa. Two-photon mechanism of particle production by high-energy colliding beams. Phys.Rev. D4, 1532 (1971).
- [34] V. B. Berestetskii, E. M. Lifshitz, L. P. Pitaevskii. Kvantovaya Elektrodinamika. — Moscow: Fizmatlit, 2001.
- [35] M. Dyndal, L. Schoeffel. The role of finite-size effects on the spectrum of equivalent photons in proton-proton collisions at the LHC. Phys.Lett.B 741, 66 (2015). [arXiv:1410.2983](#)
- [36] H. de Vries, C. W. de Jager, C. de Vries. Nuclear charge-density-distribution parameters from elastic electron scattering. Atomic Data and Nuclear Data Tables 36, 495 (1987).
- [37] G. Fricke, C. Bernhardt, K. Heilig, L. A. Schaller *et al.* Nuclear ground state charge radii from electromagnetic interactions. Atomic Data and Nuclear Data Tables 60, 177 (1995).
- [38] K. Hencken, E. A. Kuraev, V. G. Serbo. Exclusive and inclusive muon pair production in collisions of relativistic nuclei. Phys.Rev. C75, 034903 (2007).
- [39] A. J. Baltz. Higher order QCD calculations of ultrarelativistic heavy ion production of $\mu^+\mu^-$ pairs. Phys.Rev C80, 034901 (2009). [arXiv:0901.0891](#)
- [40] U. D. Jentschura, V. G. Serbo. Nuclear form factor, validity of the equivalent photon approximation and Coulomb corrections to muon pair production in photon-nucleus and nucleus-nucleus collisions. Eur.Phys.J. C64, 309 (2009). [arXiv:0908.3853](#)
- [41] S. R. Klein, J. Nystrand, J. Seger, Yu. Gorbunov, J. Butterworth. STARlight: A Monte Carlo simulation program for ultra-peripheral collisions of relativistic ions. Comm.Phys.Comm. 212, 258 (2017).
- [42] Particle Data Group. Review of Particle Physics. Chinese Physics C 40, 100001 (2016).
- [43] S. Pacetti, R. B. Feroli, E. Tomasi-Gustafsson. Proton electromagnetic form factors: basic notions, present achievements and future perspectives. Phys.Rep. 550, 1 (2015).
- [44] B. Dreher, J. Friedrech, K. Merle, H. Rothhaas, G. Lühns. The determination of the nuclear ground state and transition charge density from measured electron scattering data. Nucl.Phys. A235, 219 (1974).
- [45] A. I. Akhiezer, V. B. Berestetskii. Kvantovaya Elektrodinamika. – Moscow: Nauka, 1969. [in Russian].